IR RADIANCE MODEL VALIDATION BY SENSOR FLIGHT MEASUREMENTS

R. Baldassini Fontana
Officine Galileo, Florence, Italy

D. Sciacovelli
European Space Technology Centre (ESTEC), Noordwijk, The Netherlands

L. Fraiture
European Space Operations Centre (ESOC), Darmstadt, W.-Germany

ABSTRACT

This paper deals with the assessment of infrared radiance models of the Earth when applied to sensor calibration. The sensors considered are infrared pencil beams mounted on spinning satellites. The study is performed by comparing flight measurements of the transfer orbits of GEOS2 and OTS with simulated measurements. The model involved in the simulation describes the optics, the detector and the electronics of the pencil beams based on directly measured parameters and laboratory test data. The radiance models whose merits are scrutinised are the NASA model and the BAC-ESRO IV model. Both are found to be equally good in the investigation which has been conducted.

1. INTRODUCTION

Infrared (IR) sensors are commonly used on spin stabilised satellites to provide attitude information based on the detection of the earth infrared horizon located at approximately 40 km above the solid earth. The wavelength of operation of these sensors is generally limited to the region of CO_2 emissivity, i.e. 14:16.25 μ. This spectral band is not influenced by the atmospheric weather conditions and diurnal variations. Sensor measurements are known to have sizable delays which have to be assessed and compensated before the attitude reconstruction is attempted. The effects of the long term variations (seasonal) on the attitude sensor measurements are analysed in the following using the two known models of the earth radiance. One of these is the analytical model which was derived from data of an IR experiment flown on the ESA-ESRO IV satellite in 1974 (ref.1) and (ref.4). The other model has been established in a NASA paper (ref. 3).

Only IR sensors of the pencil beam type are considered. They consist of two narrow beam telescopes strapped down to the satellite. The OTS sensor for which the two IR telescope lenses and the V-beam Sun sensor slits are visible, is shown in figure 1.1.

The sensor rotates with the satellite and each telescope or beam of the sensor delivers a pulse at the space/earth (S/E) and the earth/space (E/S) transition of the field of view across the IR-earth limb.

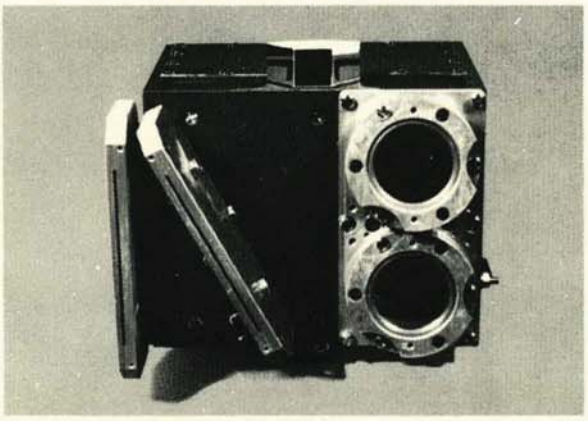

Figure 1.1 The OTS elevation sensor (OG/ESS-02) built by Officine Gallileo in Florence

The detection if accomplished by a Germanium immersed bolometer collecting the incoming IR energy, followed by a signal processing system sensing the signal edge transitions. Nominally the measurements are defined when the "line of sight" of the telescopes crosses the geometrically defined apparent earth disc. Many errors are occurring during the detection process. They are related to the IR radiance definition, the misalignments in the sensor mounting, the line of sight definition and the delay occurring in the signal processing unit. Directly measurable components of the errors are calibrated on ground. The remaining error consists of a bias and a random component. The major contribution to the bias error comes from the IR earth radiance variation.

It is impossible to simulate the full range of transfer orbit conditions in laboratory tests of the IR sensors. Therefore it has been decided from the ESA satellite GEOS1 onwards to enable the production of calibration data by means of a digital computer simulation program. To this aim a detailed mathematical model of the sensor has been developed and then validated against laboratory test data. In the latter a homogeneous IR radiance over the earth disc has been represented by a heated disc and the disc itself has been shaped to represent the earth seen at geostationary altitude. Once validated, the simu-

Proc. Int. Symp. Spacecraft Flight Dynamics, Darmstadt, FRG, 18-22 May 1981 (ESA SP-160, Aug. 1981)

lation program allows the production of calibration data for arbitrary orbits, spin rates and attitudes without additional hardware testing.

In the study described in this paper, the simulation program has been used to evaluate the effect of different IR-radiance models when compared to the actual flight measurements of GEOS 2 and OTS. Before that comparison is made, the background material is described. It comprises the sensor operation principles, their mathematical modelling, the two IR-radiance models, the nature and context of the "in-flight" measurements and the actual attitude and orbit parameters of GEOS 2 and OTS.

2. SENSOR OPERATION

2.1 Sensor Configuration

A pencil beam infrared sensor block consists of two static IR telescopes. The output of the latter is fed into a processing electronics which transforms the output signal into logic pulses occurring at the space/earth (S/E) and earth/space (E/S) transitions. The two beams have their pointing axis lying in a meridian plane of the satellite at an angle ξ_i (i=1,2) from the spin axis (see figure 2.1.1). The values of ξ_i are selected to satisfy the earth coverage requirements.

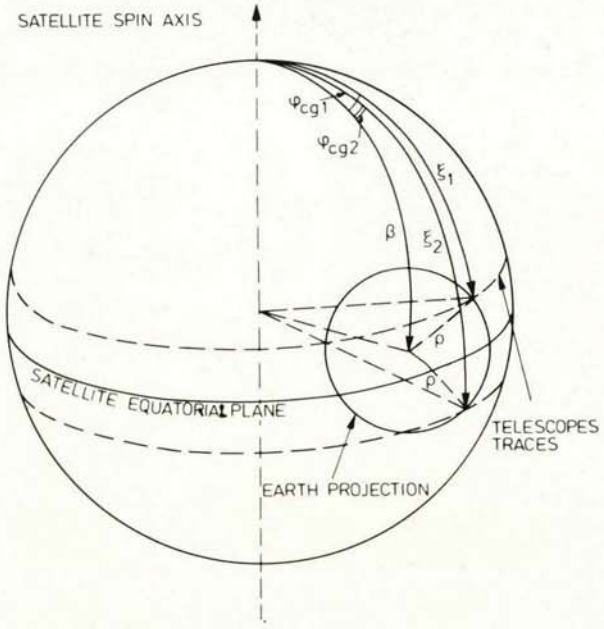

Figure 2.1.1 Dual beam infrared sensor configuration inside a spinning satellite

The earth aspect angle β, the swept geometric chord $\phi_{c,g}$, the telescope inclination ξ_i and the earth apparent diameter 2ρ, are related by the equation :

$$\cos\left(\frac{\phi_{c,g}}{2}\right) = \frac{\cos\rho - \cos\beta\cos\xi_i}{\sin\beta\sin\xi_i} \quad (i=1,2)$$

The sensor measures the electronic crossing phases $\phi_{se,e}$ and $\phi_{es,e}$ corresponding to the S/E and E/S transitions with respect to a reference signal coming from a sun sensor slit (figure 2.1.2). If both telescopes have coverage (=sense the earth) the two measurements of the electrical chords

$$(\phi_{c,e})_i = (\phi_{es,e} - \phi_{se,e})_i \quad (i = 1,2)$$

allow the computation of the earth colatitude without the intervention of the earth apparent radius ρ.

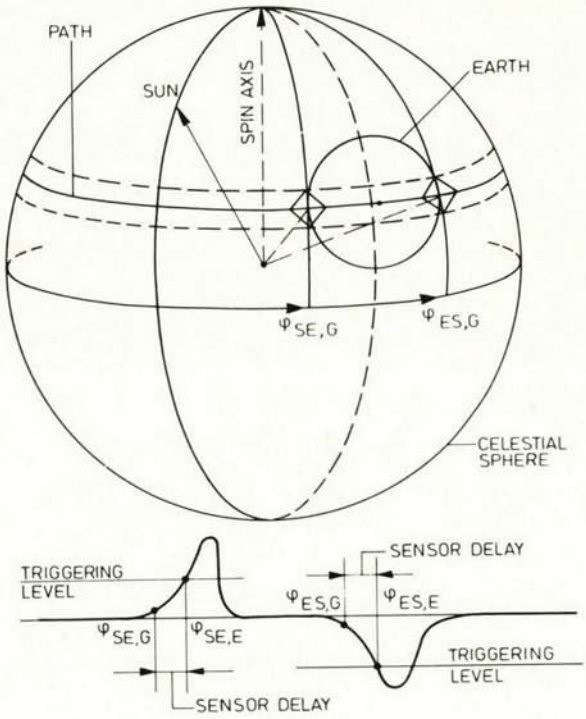

Figure 2.1.2 Earth sensor geometric and electronic-triggering phases for one beam

To achieve full redundancy of operation the IR beams are optically and electrically independent. Each infrared telescope consists essentially of:

- a germanium objective; this optical part is coated for antireflection in the spectral region of interest, i.e. 14 to 16.25μ
- an interferential optical filter limiting the transmitted radiation band to the chosen spectral region
- an immersed thermistor bolometer giving a square shaped nominal Field Of View (F.O.V.)
- a sun guard sensor aligned parallel to the optical axis of the IR telescope

The processing electronics of each beam is based on a derivator concept associated to peak detection and percent threshold setting. It consists of the following main block functions (see figure 2.1.3):

- low noise preamplifier,
- one band pass filter to differentiate the earth detection signal and to eliminate low and high frequency noise,
- two peak detector circuits to which the leading and trailing edge signals (corresponding to S/E

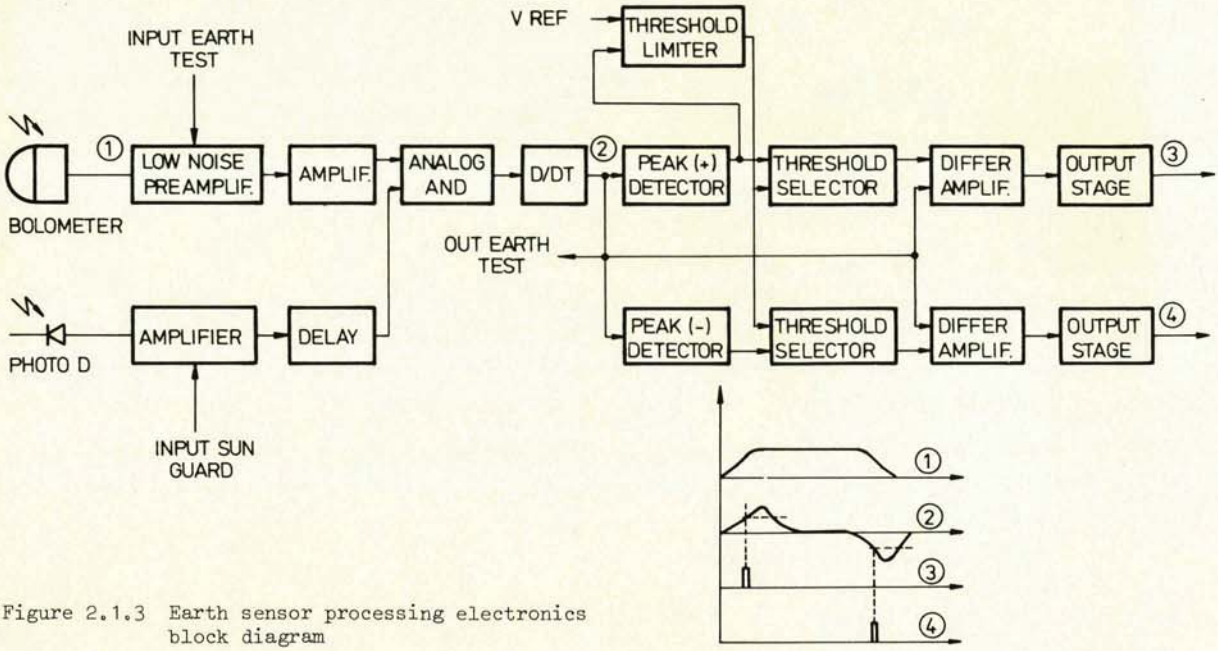

Figure 2.1.3 Earth sensor processing electronics block diagram

and E/S radiance gradients) are fed. The triggering level for the crossing information is set to a fixed percentage of the signal amplitudes obtained by the derivators. This triggering level setting is chosen to counteract the seasonal variation of earth radiance,

- two different amplifiers to which the outputs from the derivators and the triggering levels are fed

- an absolute minimum threshold to avoid output signals due to noise in the absence of the earth in the F.O.V. of the IR telescope.

The IR channel operation is temporarily disabled when the sun enters the field of view of the sun guard sensor. The time interval during which the sensor is inoperative is determined by a proper delay circuit.

2.2 Mathematical Model and Parameters affecting the Sensor Measurements

The actual sensor measurements are the crossing phases defined at the instant when the electronic output signal transgresses the threshold level which is normalised to a specific percentage of the maximum output signal. This triggering mechanism is independent for the leading (S/E) and trailing (E/S) transition pulses. As previously mentioned, leading and trailing phases are measured with respect to a sun pulse occurrence. This is accomplished by datating IR pulses with respect to the sun presence pulse corresponding to the instant when the sun crosses the meridian slit. This slit is part of the IR sensor unit for OTS, while it is indirectly connected to the IR sensor for GEOS 2.

The ideal sensor measurements are the geometric phases defined in figure 2.1.2 when the optical axis is tangent to the earth surface. The ideal sensor measurements are functionally dependent upon the ideal spin axis attitude, the earth view angle and the mounting geometry. This is also true for the physical measurements which moreover are also influenced by a number of unknown or partly known parameters such as misalignments, bolometer responsivity, electronic time constants and earth radiance profile. The relative importance of these parameters with respect to their influence on the IR measurements is ascertained by evaluating the sensitivity of the attitude residuals to parameter variations. Attitude measurement residuals are defined as the difference between simulated or in-flight sensor

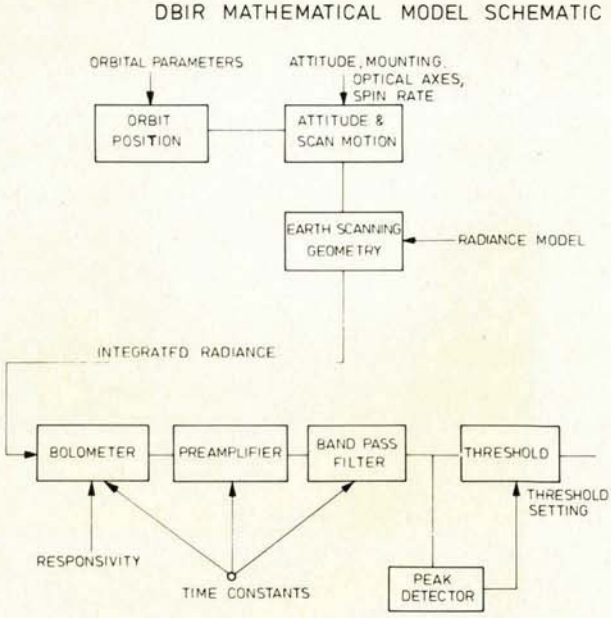

Figure 2.2.1 IR pencil beam sensor simulation flow-chart

measurements minus the geometrically ideal measurements. Thus, two kinds of residuals are considered : the residuals of the simulated model and the residuals of the actual in-flight data or the experimental residuals.

The sensor model has to take into account all parameters which may influence the physical result of the measurement process. A scheme of the model which has been programmed, is shown in figure 2.2.1. It considers the following parameters :

- the sensor internal and external alignments
- the focal length and the lens radius for the optical head
- the bolometer shape and responsivity
- the electronic transfer function and its time constants
- the limb crossing geometry and the collection of the IR radiation affected by the IR earth radiance model.

The computer program first analyses the crossing of the F.O.V. with the earth IR limb as function of orbit and satellite attitude. This is the start point to compute the integrated energy at the input of the bolometer. At a number of discrete scanning angle values the geometrically defined earth is projected on the detector plane and the common area between detector and earth disc is computed. At these points the model earth IR radiance for the relevant earth latitude is computed and inserted.

The integration process at the input of the electronic transfer function assumes a linear interpolation between these discrete points. Closed form expressions are the basis for determining the electronics output signal and derivatives. An iterative procedure is implemented for determining the maximum signal, the threshold level and the threshold crossing phases. A detailed description of the mathematical relations and of the computational methods is given in Ref. 2 .

The simulation program allows the evaluation of "modelled" sensor residuals for any set of given parameters. It also permits to assess the measurement-residual-sensitivity with respect to parameter variations. The corrective terms derived by means of the model, which account for a known set of parameters can be considered as a calibration table. During the satellite flight, calibration data for a modified orbit, spin rate and attitude can promptly be generated to cope with the actual conditions.

Distorsions of the in-flight residuals with respect to the simulated ones for actual flight conditions may give information about "a priori" unknown parameters such as earth radiance seasonal variations. In fact, results of simulations which account for earth radiance models may be compared with in-flight data, thus giving a capability of validation.

The simulation model requires that sensor parameters as detector responsivity, optical axis geometry, electronic time constants and triggering levels are known. Detector responsivity and triggering levels are measured in the laboratory. The nominal values of electronic time constants are usually accurate enough to be inserted as such, while the optical axis inclination is

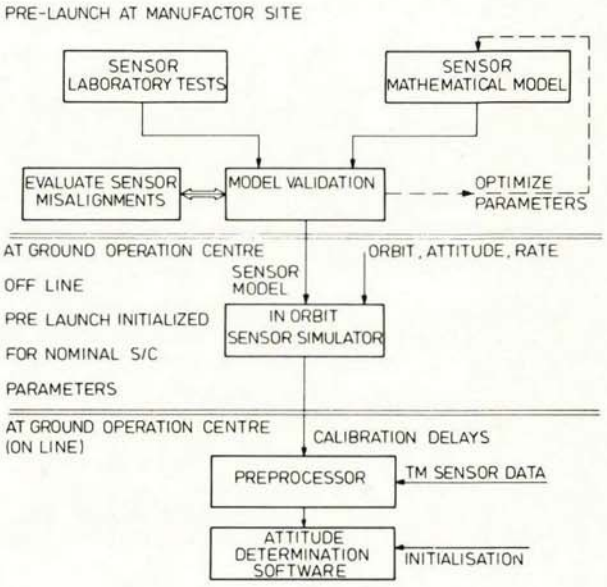

Figure 2.2.2 Overall IR-sensor calibration procedure

optimised by means of computer runs to fit results of laboratory tests performed with the complete sensor unit on a spin table.

If all the parameters typical for a given sensor are available, the simulation program can be operated to produce flight calibration data. The whole procedure of assessing the model parameters and its final utilisation in operations is shown figure 2.2.2.

As an example, graphs of simulated GEOS attitude measurement residuals are grouped in the figures 2.2.3 through 2.2.6. They give an idea of the residual sensitivity with respect to attitude parameter variations. In figure 2.2.3 the nominal case is shown. Figure 2.2.4 shows the residual variation for a $\pm 1^{\circ}$ offset in spin axis right ascension. In figure 2.2.5 the effect of a $\pm 0.5^{\circ}$ change in spin axis declination is given and in figure 2.2.6 the effect of a spin axis tilt of 1° in the satellite body is plotted.

These figures are added at the end of this paper.

For the present earth radiance model validation study only data are considered for which the absolute spin axis direction is known to an error of at most 0.1° as derived from apogee motor firing assessment calculations. Moreover, a spin axis tilt of less than 0.1° has been included to allow for a small spacecraft unbalance not excluded by the overall satellite specification.

2.3 Earth Radiance Models

The detector output signals are affected by earth radiance variations in the working wavelength band (14 : 16.25μ). If the sensor simulation model has to produce accurate calibration data, it is essential that the earth radiance model is sufficiently realistic. Only two models are

described in the accessible literature : the NASA-model (ref.3) and the BAC-ESRO IV model (ref.1). Both are considered and a summary of them is given hereafter.

2.3.1 NASA Model

In the early days of space technology the wavelength choice for earth horizon detection has been supported by theoretical and experimental studies carried out in USA(ref.3).Thereby it has been concluded that the detection of the earth horizon within the 14-16.25μ band is not seriously affected by atmospherical conditions while a seasonal effect is present inside the earth disc showing monotonic decreases of radiance from the hot pole to the cold pole. No diurnal variations have appeared for East-West scanning throughout the seasons. The same report (ref.3) also gives the radiance profiles at the horizon in function of latitude and search.

The radiance model for the inner earth disc can be summarised in the following table giving radiances in μWatt per m^2 ster.

Latitude	Northern Winter Solstice	Equinox	Northern Summer Solstice
70°	4.26	5.5	6.76
60°	4.6	5.5	6.5
50°	4.7	5.5	6.4
40°	4.8	5.5	6.2
30°	5.0	5.5	6.0
20°	5.2	5.5	5.7
10°	5.2	5.5	5.6
0°	5.5	5.5	5.5
-10°	5.6	5.5	5.2
-20°	5.7	5.5	5.2
-30°	6.0	5.5	5.0
-40°	6.2	5.5	4.8
-50°	6.4	5.5	4.7
-60°	6.5	5.5	4.6
-70°	6.76	5.5	4.26

The simplifying assumptions are that summer and winter are antisymmetric in radiance behaviour (neglecting the perihelion and aphelion effects) and that no delays are involved i.e. the maximum radiation at the North pole exactly occurs at the summer solstice. The radiances at other dates can be obtained by interpolation.

2.3.2 ESA Model

More recently BAC has derived a mathematical model from ESRO IV data(ref.1).This model approximates the radiance variations with an analytical function of latitude and time of year by means of the relationship :

$\theta < \theta_m$:

$$R = 5.0 + 2.6\{\sin^2\{\frac{\pi(\theta-\theta_m+12.5)}{90+\theta_m-12.5}\} - \sin^2\{\frac{\pi 12.5}{90+\theta_m-12.5}\}\}.\ f_1(t)$$

$\theta > \theta_m$:

$$R = 5.0 - 1.9\{\sin^2\{\frac{\pi(\theta-\theta_m-12.5)}{90-\theta_m-12.5}\} - \sin^2\{\frac{\pi 12.5}{90-\theta_m-12.5}\}\}\ .f_2(t)$$

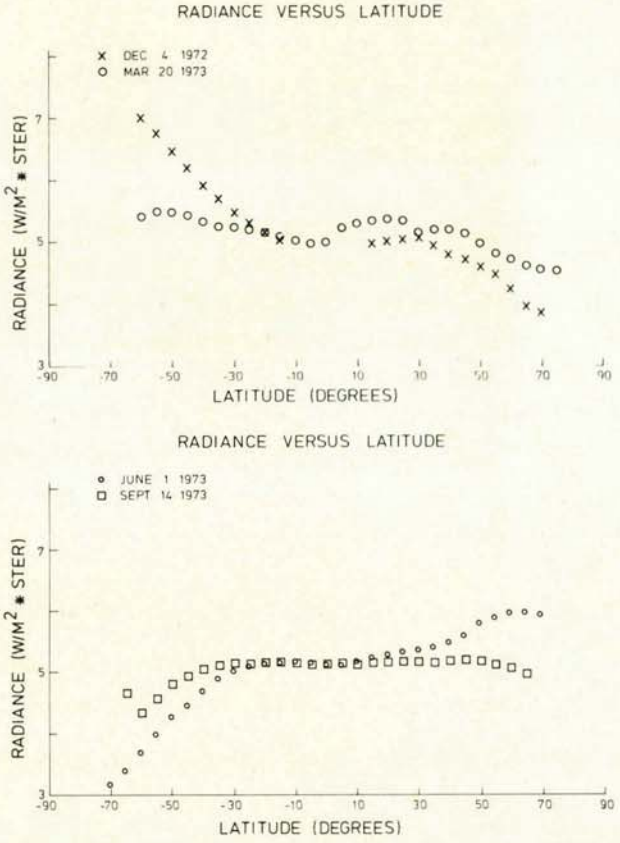

Figure 2.3.1 IR earth radiance versus latitude

where :

$\theta_m = 2.5^\circ + 10^\circ \cos(\frac{\pi t}{6})$

$f_1(t) = \cos(\frac{\pi t}{6})$

$f_2(t) = 1 - t/3$, for $t < 6$; $t/3 - 3$, for $t > 6$

θ represents the latitude from -90° to $+90^\circ$

t stands for the time of the year in months, i.e. Jan 1st = 0.0 and Dec 31st = 12.0

R is the radiance ($\mu W/m^2$ x ster)

Earth radiance variations versus latitude for different times of year are depicted in figures 2.3.1 as deduced from this model.

3. ANALYSIS OF THE IN-FLIGHT MEASUREMENTS

The flight data have been collected during the last parts of the transfer orbits of OTS and GEOS 2. The spacecraft attitude between the last attitude reorientation manoeuvre (over less than 1°) and the apogee motor firing can be recomputed 'a posteriori' to an absolute accuracy of $\pm 0.1^\circ$ by means of trajectory performance figures. As announced earlier, also a spin axis tilt of at most 0.1° has to be considered as possible. Both uncertainties : attitude knowledge and rotation axis tilt, define a band around the simulated residuals in which the flight residuals should be contained if no unknown systematic effect influences the pencil beam measurements.

The in-flight residuals have been derived from the datated attitude measurements archived by ESOC. They contain chords, leading and trailing phase data. The mathematical model provides the simulated residuals by using the available earth radiance models, the sensor parameters and the assessment of the actual attitude and orbit.

3.1 The Satellites and their Attitude Flight Measurements

Both, OTS and GEOS 2 are designed to downlink the attitude measurements in digital form merged in a fixed length telemetry format. This was and will remain the standard for ESA transfer orbit spinners. In this subsection, it is described in short how and with which frequency the measurements are sampled in the two satellites considered.

In the OTS case, there is only one sensor block containing IR pencil beams of the type described in section 2 and shown in figure 1.1. Their declination with respect to the spacecraft equator is 6° and 10°, omitting the fine alignment corrections. The attitude measurements are sampled in parallel. They are represented without commutation in the telemetry format, i.e. always at the same format address with the same meaning. Parallel means that the sampling mechanism aims at obtaining all measurements within approximately one spin period.

Explicit figures to the OTS attitude measurement onboard sampling and encoding. In the transfer orbit, the target spin rate is 60 rpm. With that figure in mind, the basic sampling period has been selected to 1.6 sec. The attitude measurement electronics consists of two units each having a 16 bit clock or counter driven at 20,480 Hz and 3 registers. Both clocks are synchronised at the start time of the format and are reset at full count (3.2 sec). As a full telemetry format lasts 25.6 sec, there are just 8 full counts of the attitude measurement clocks.

The arrival of the meridian sun sensor slit pulse, the skew sun sensor slit pulse, the S/E pulse and E/S pulse of the 4° and 10° pencil beam sensors, causes the clock content to be copied in one of the six dedicated registers. This register contents are sampled once (sun sensor slits and 10° beam) or twice (6° beam) per 1.6 sec and sent to the ground in the housekeeping telemetry format.

The conclusion is that for OTS the quantisation interval of a single pulse is 0.018° meaning a $\pm 0.009^{\circ}$ worst case accuracy. An angle is constructed from two pulses and therefore the whole sampling mechanism gives rise to a rectangular distributed noise interval $\pm 0.018^{\circ}$.

For GEOS2 there are two sensor blocks of 2 pencil beams each. They are redundant units and only one block has been operated throughout the transfer orbit. The declination of the beams is plus and minus 6° with respect to the s/c equator apart from the alignment errors. The attitude measurement is serial and compared to OTS where pulse occurrences as such are registered, GEOS 2 produces counts measuring the interval between two predefined pulses. There are eight of such start and stop pulse combinations (spin period, spin phase, sun colatitude, earth chord and sun to S/E for each telescope and sun to E/S for only one telescope.

A new measurement can only be taken if the previous one has been telemetered. This means that a full cycle of 8 measurements can repeat at the earliest every 8 spin periods. In the transfer orbit the commutated attitude measurement is sampled only every 1.38 sec. At 90 rpm the latter frequency decides on the actual sampling frequency of a given measurement type. It is in the best case $8 \times 1.38 \simeq 11$ sec. The clock frequency during the count is 47.625 Hz for the transfer orbit spin rate. The quantisation causes a possible error at the count start and stop which amounts to maximum twice the quantisation interval itself. At 90 rpm this is 0.023° which gives rise to a rectangular distributed noise of $\pm 0.011^{\circ}$ if the measurements are well-preprocessed.

Thus, the attitude measurement systems for OTS and GEOS 2 though very different in the sampling mechanism and frequency, produce measurements with nearly equal accuracy.

3.2 Operational Aspects

The infrared pencil beam sensors are the conventional attitude measurement devices for spinning satellites during transfer orbits (TO). Typical for such a TO is that a solid propellant kick motor has to be fired either at perigee or apogee. The latter is the more frequent case because it is used to bring spacecraft into a geosynchronous orbit. This is also the case for GEOS 2 and OTS. The satellite attitude knowledge accuracy before the motor firing should always be better than 1°. The origin of this requirement is beyond the scope of this paper.

During the transfer orbit the IR-pencil beam measurements have to be processed together with the sun sensor data in order to obtain attitudes.

The ESA procedure is to manoeuvre as close as 0.5° to the ideal motor direction by means of an hyperfine manoeuvre not too long before the motor firing. The attitude knowledge just before the hyperfine manoeuvre should have the best possible accuracy (maximum error $\sim 1^{\circ}$). As the infrared sensor calibration is orbit, spin rate, attitude and season dependent, it is reasonable to update the IR-pencil beam calibration during TO.

The sequence of ground-based-activities before the hyperfine manoeuvre is :

- attitude measurement preprocessing with addition of some nominal calibration corrections
- attitude estimations
- production of a new set of calibration data on the basis of the actual attitude and spin rate
- new preprocessing and estimations
- residuals analysis to select manually the best attitude estimate among slightly different alternative results

The ability of producing calibration data sets more or less on line has numerous advantages :

- the attitude estimation accuracy is guaranteed for any non-nominal feature in the TO trajectory, attitude or spin rate (GEOS 1 is a good example)

- the calibration in the laboratory and the production of an initial calibration data set has not to cope with any launch delays. These delays cause the calibration values to change due to the seasonal IR earth radiance pattern variation.

3.3 OTS Transfer Orbit and in-flight Data Analysis

OTS satellite parameters in transfer orbit concerning the time ranging from the end of the hyperfine manoeuvre to the apogee motor firing are summarised in the following table :

OTS transfer orbit		
Apogee altitude		35778.565 km
Perigee altitude		184.534 km
Right ascension of ascending node		32.821 deg
Perigee argument		179.727 deg
Orbit inclination		27.354 deg
Launch date		13/05/1978
Spin axis right ascension		121.600 deg
Spin axis declination		-24.000 deg
Spin rate		60.66 rpm
(Coverage span	Telescope 1	139÷176 deg
(in true anomaly	Telescope 2	152÷180 deg

The OTS infrared sensor in-flight residuals are reported in the figure 3.3.1. In figure 3.3.2 the area of uncertainty is indicated. It results from an assumed error of $\pm 0.1^{\circ}$ in the spin axis orientation, of 0.1° in tilt and of $\pm 0.1^{\circ}$ in the inclination of the telescope optical axis. In figure 3.3.3 the residuals corresponding to the radiance models under study are given. As previously mentioned, chord residuals are the differences between in-flight chord measurements and the simulated chord angles. The leading and trailing residuals are defined in the same way.

The sum of all azimuth misalignments on each optical beam axis yields an unknown constant delay of the same sign on both leading and trailing measurements, while it has no effect on the chord measurements. The misalignments in the optical axis elevation leads to a non-uniform distorsion of the residuals. Residual plots showing this distorsion in an exaggerated fashion are given in figure 2.2.6.

Error sources contributing to the azimuth positioning are sensor internal misalignments, azimuth alignments between the sun sensor and the IR sensor unit and a meridian sun pulse delay. The delay of the meridian sun sensor pulse has been assessed to be less than 0.05°. The overall unknown azimuth misalignment is estimated less than 0.1° corresponding to about 0.3 m sec. on the measured leading and trailing phases.

The accuracy by which the telescope optical axis inclination is known is hypothised to be better than $\pm 0.1^{\circ}$. This value is based on the experience gained in applying the pre-flight calibration procedure described in section 1.2. The spin axis orientation knowledge and the spin axis tilt both may be in error by 0.1° as explained in the beginning of section 3.

The data analysed in figures 3.3.1 to 3.3.3 are taken from the sensor earth coverage period in the last orbit prior to apogee motor firing. During this period of coverage a hyperfine attitude manoeuvre has been performed. The satellite is there approximately at 150° true anomaly. The effect of this manoeuvre can be seen in the small discontinuity in the residuals in figure 3.3.1.

The approach followed in the analysis has been in the first instance to fit the in-flight residuals to the simulated strip of uncertainty and then to the curves obtained for the two different radiance models : NASA and ESA. In general good agreement was found between predicted and in-flight residuals for both radiance models. It can be noticed that near the equinox both models lead to very similar residuals. Having this in mind the following remarks can be made on the basis of the results depicted in figures 3.3.1.

Telescope 1

The in-flight residuals for the leading phase lie between the two curves describing simulated residuals together with these obtained by employing ESA and NASA models, with a mean uncertainty less than 0.3 msec.

The in-flight residuals for the trailing phase are very near to the NASA model, i.e. not worse than 0.2 msec. Both models ESA and NASA are however in the area of uncertainty defined in figure 3.3.2.

The in-flight residuals for the chord are in the area of uncertainty of figure 3.3.2. Residuals for non-homogeneous radiance, either ESA and NASA, both fall in the area of uncertainty.

Telescope 2

The in-flight residuals for the leading phase tend to the ESA and NASA residuals in the second part of the coverage, namely between 163° and 180° of true anomaly. Better agreement would be reached if the actual telescope inclination differs by -0.1° from the value used in the computer simulator to find the geometrical and simulated phases.

The in-flight residuals for the trailing phase: the same observations made for the leading phase residuals are valid.

The in-flight residuals for the chord phase : the observations made before apply.

3.4 GEOS 2 Transfer Orbit In-flight Data Analysis

GEOS 2 transfer orbit parameters are summarised below for the time interval following the hyperfine manoeuvre up to the apogee motor firing.

GEOS 2 Transfer Orbit		
Apogee altitude		35 542.262km
Perigee altitude		210.96 km
Right Ascension of Ascending Mode		271.76 deg
Argument of perigee		179.538 deg
Orbit inclination		25.841 deg
Launch date		15/07/1978
Spin axis right ascension		181.340 deg
Spin axis declination		22.980 deg
Spin rate		94.77 rpm
Coverage span	Telescope 1	176:206 deg
in true anomaly	Telescope 2	153:183 deg

The GEOS 2 infrared sensor in-flight residuals are reported in the figure 3.4.1. Similar to the OTS case on figure 3.4.2 the area of uncertainty which results from a possible error of $\pm 0.1^{\circ}$ in the spin axis direction, tilt or optical axis inclination is indicated. For the two radiance models under study the residuals obtained by simulations are shown in figure 3.4.3.

The considerations made concerning the azimuth misalignment in the OTS case remain valid as well as the uncertainty band around the nominal values of the residuals. GEOS 2 has a spin rate of 99.77 rpm and therefore a turn of 0.1° is made in 0.18 m sec.

From a first visual inspection of the residuals it can be said that a good agreement between in-flight and simulated data is obtained for telescope 1, while for the telescope 2 the fitting between in-flight and simulated data is not satisfactory. In trying to find the reason for this difference it has not been possible to identify a change of a parameter, or a realistic earth radiance profile which satisfactorily explains the observed discrepancy. A possible explanation is a non-optimal value of the optical axis inclination of the telescope 2 in the order of 0.2° to 0.3°. This could result from a non-uniform distribution of responsivity on the detector sensitive area. A reconsideration of the achieved pre-flight calibration accuracy for telescope 2 tends to confirm this possibility.

In the case of GEOS-2 the radiance variations are a significant cause of shift of the residuals from their nominal values. This is due to the fact that the measurements are made during the month of July when the radiance energy has its maximum value in the Northern hemisphere and its minimum value in the Southern hemisphere. For the given spin rate direction and spin axis orientation the observed IR radiation has an important negative gradient when crossing the earth disc.

Only the in-flight measurements of telescope 1 are used for comparison purposes. The following remarks are made on the basis of the results depicted in the figures 3.4.1 to 3.4.3.

Telescope 1

The in-flight residuals for the leading phase are close to both ESA and NASA simulated residuals.

The chord phase residuals follow more closely the behaviour of the ESA-BAC model simulated residuals.

4. CONCLUSIONS

The purpose of the study has been to validate an earth radiance seasonal model derived from an infrared experiment flown on the ESRO IV satellite in 1974. This ESA model is deduced by analysis of in-flight measurements. It is by 10 years younger than the NASA model based upon experiments and theoretical studies carried out in 1964.

The comparison between in-flight and simulated data, even if it does not allow to choose a best model, forms a basis for qualifying both IR earth radiance representations for describing the long term variations which may affect IR pencil beam measurements.

Besides the above conclusion it can be stated that visualising the in-flight residuals is a very useful check for validating the in-flight attitude estimate. Further this study has shown that anomalies in the pre-flight calibration can be detected 'a posteriori'. The small mismatch of the optical axis inclination of one of the two IR telescopes of GEOS 2 has been observed in this manner.

REFERENCES

1. B.A.C. ESS/SS 722, 'Modelling of the Earth Radiance from ESRO IV HCI Data', September 1976
2. ESTEC Working Paper No. 1066, 'Measurement Errors of Pencil Beam Infrared Sensors in Transfer Orbit', by D. Sciacovelli
3. NASA CR725, m,' The Analysis of 15 Micron Infrared Horizon Radiance Profile Variations over a Range of Meteorological Geographical and Seasonal conditions', April 1967
4. ESA TR-15, 'Comprehensive Report on the Horizon Crossing Indicator flown on ESRO IV' by A. S. Menardi, R. Fontana, G. Simoncini and G. Devidi, November 1977

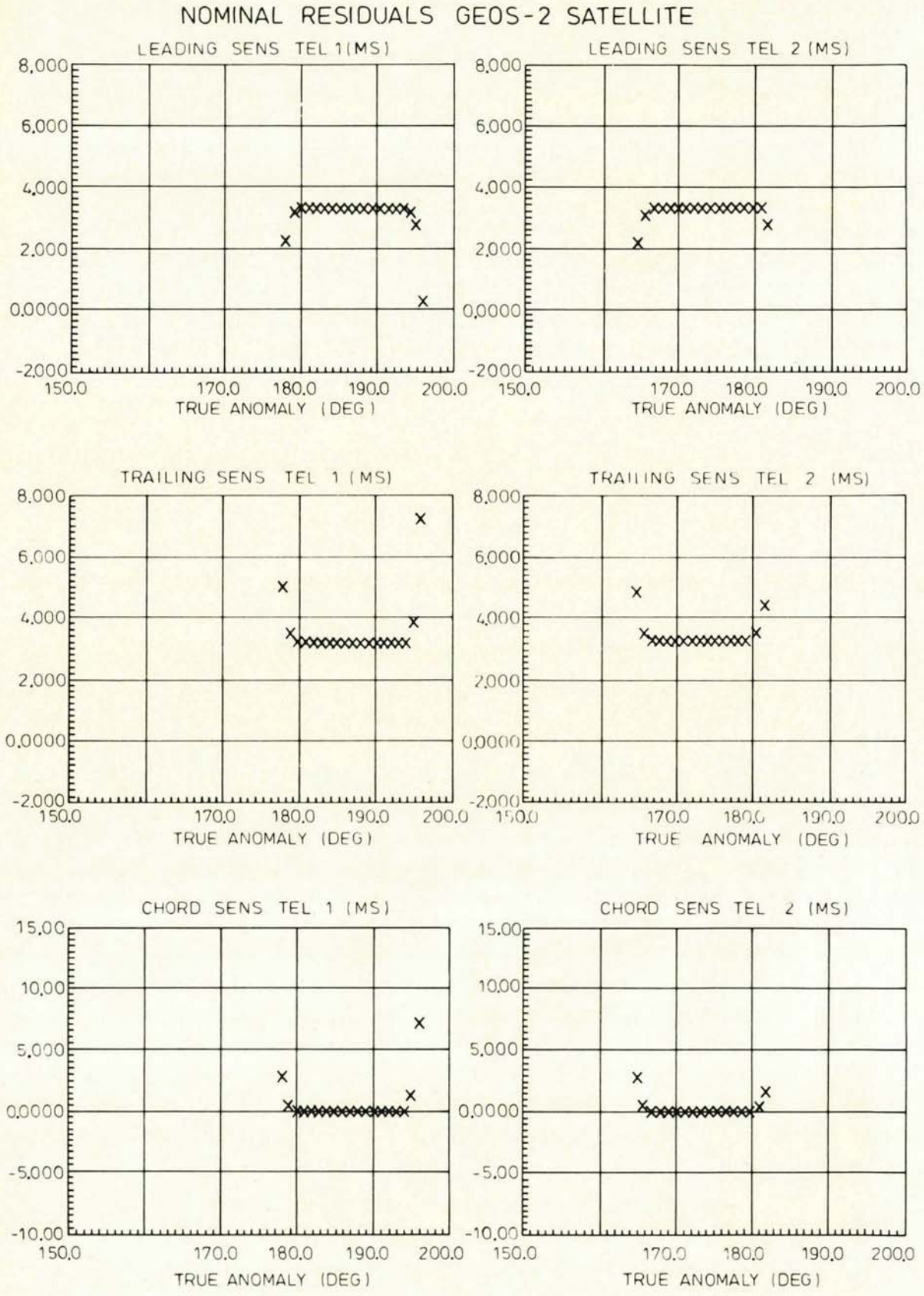
NOMINAL RESIDUALS GEOS-2 SATELLITE
LEADING SENS TEL 1(MS)
LEADING SENS TEL 2 (MS)
TRAILING SENS TEL 1 (MS)
TRAILING SENS TEL 2 (MS)
CHORD SENS TEL 1 (MS)
CHORD SENS TEL 2 (MS)
TRUE ANOMALY (DEG)
8.000
6.000
4.000
2.000
0.0000
-2.000
15.00
10.00
5.000
-5.000
-10.00
150.0
170.0
180.0
190.0
200.0

Figure 2.2.3

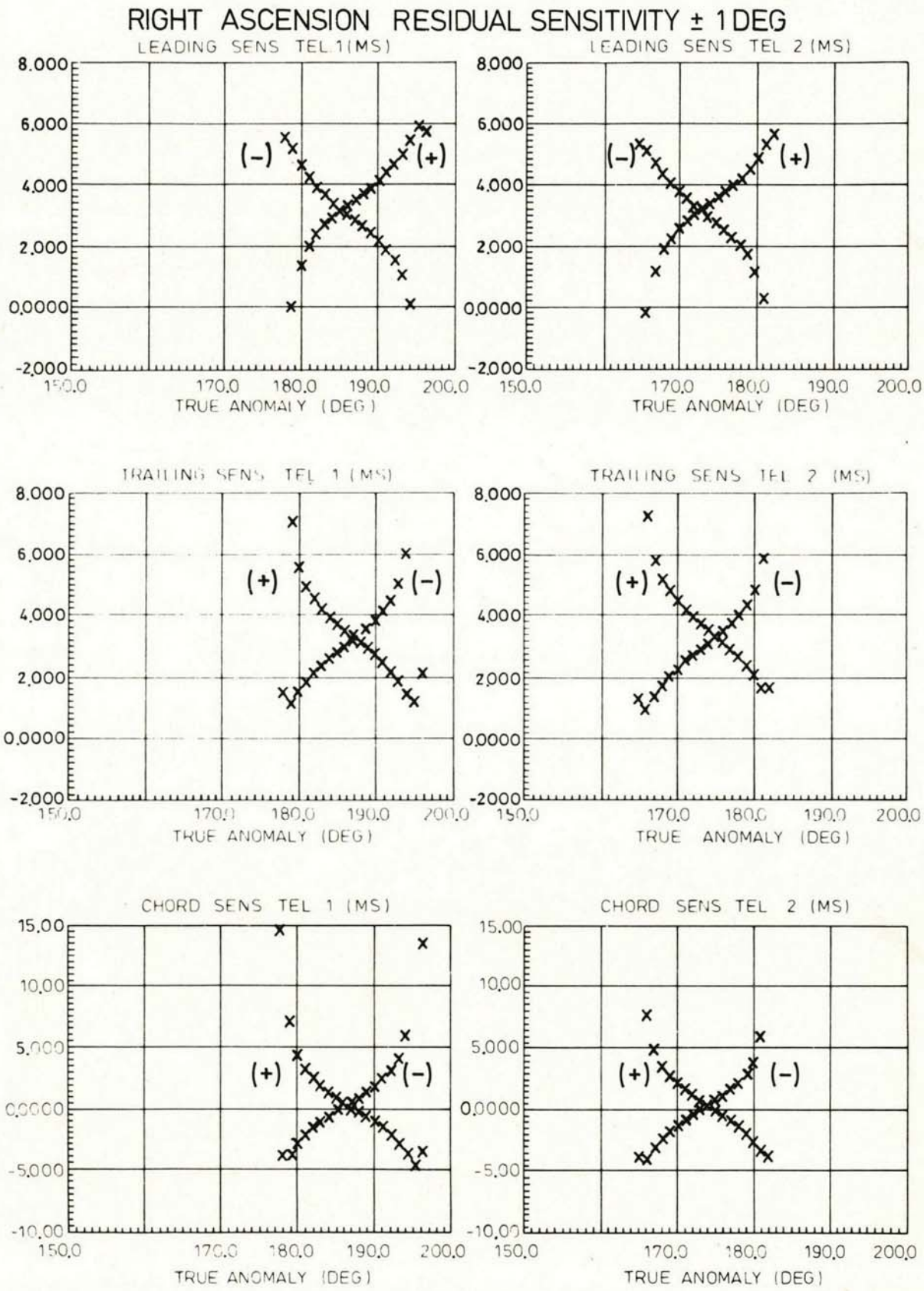
RIGHT ASCENSION RESIDUAL SENSITIVITY ± 1 DEG
LEADING SENS TEL 1 (MS)
LEADING SENS TEL 2 (MS)
TRAILING SENS TEL 1 (MS)
TRAILING SENS TEL 2 (MS)
CHORD SENS TEL 1 (MS)
CHORD SENS TEL 2 (MS)
TRUE ANOMALY (DEG)
(+)
(-)

Figure 2.2.4

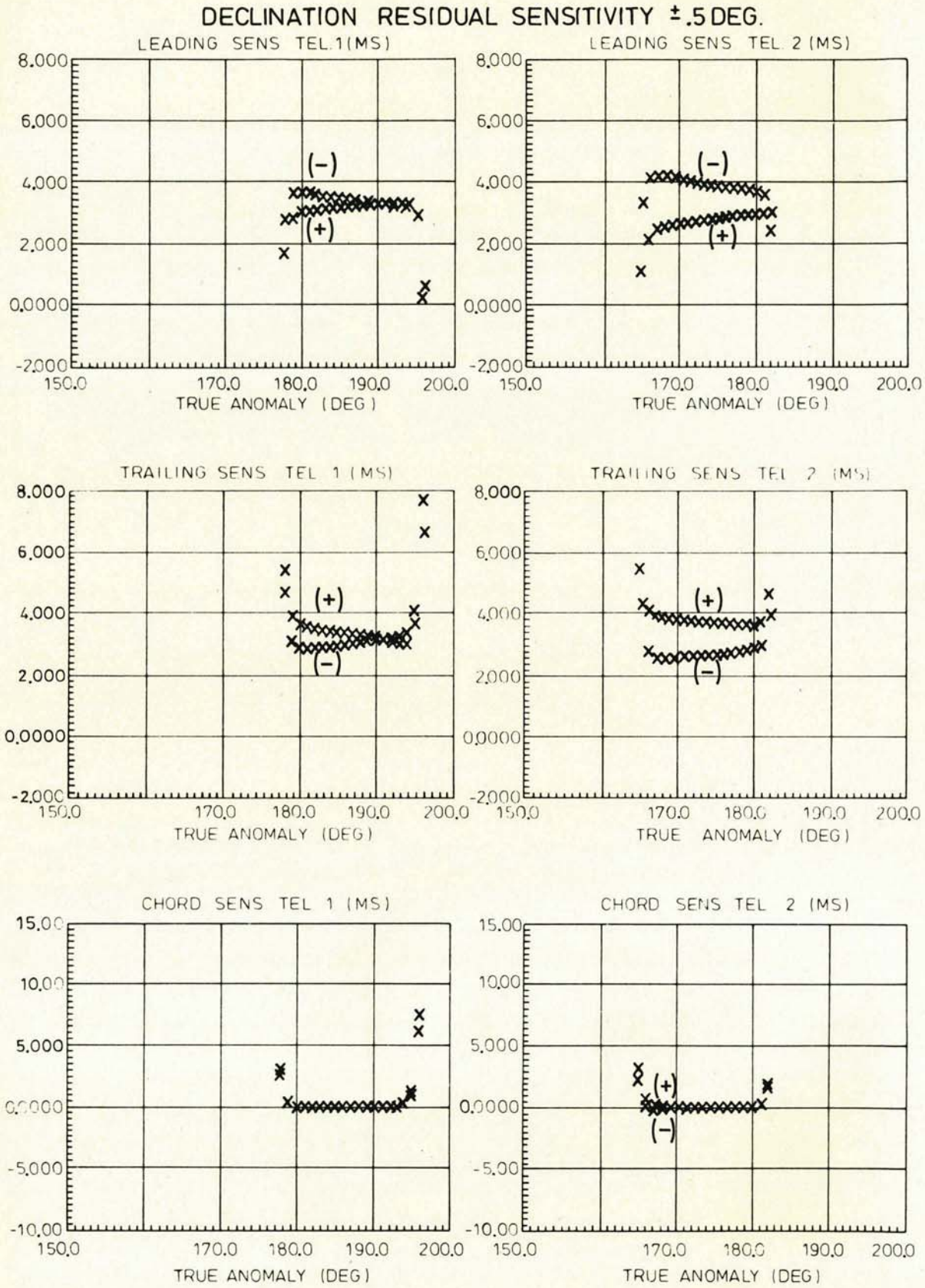
DECLINATION RESIDUAL SENSITIVITY ±.5 DEG.
LEADING SENS TEL 1 (MS)
LEADING SENS TEL 2 (MS)
TRAILING SENS TEL 1 (MS)
TRAILING SENS TEL 2 (MS)
CHORD SENS TEL 1 (MS)
CHORD SENS TEL 2 (MS)
TRUE ANOMALY (DEG)
(+)
(-)

Figure 2.2.5

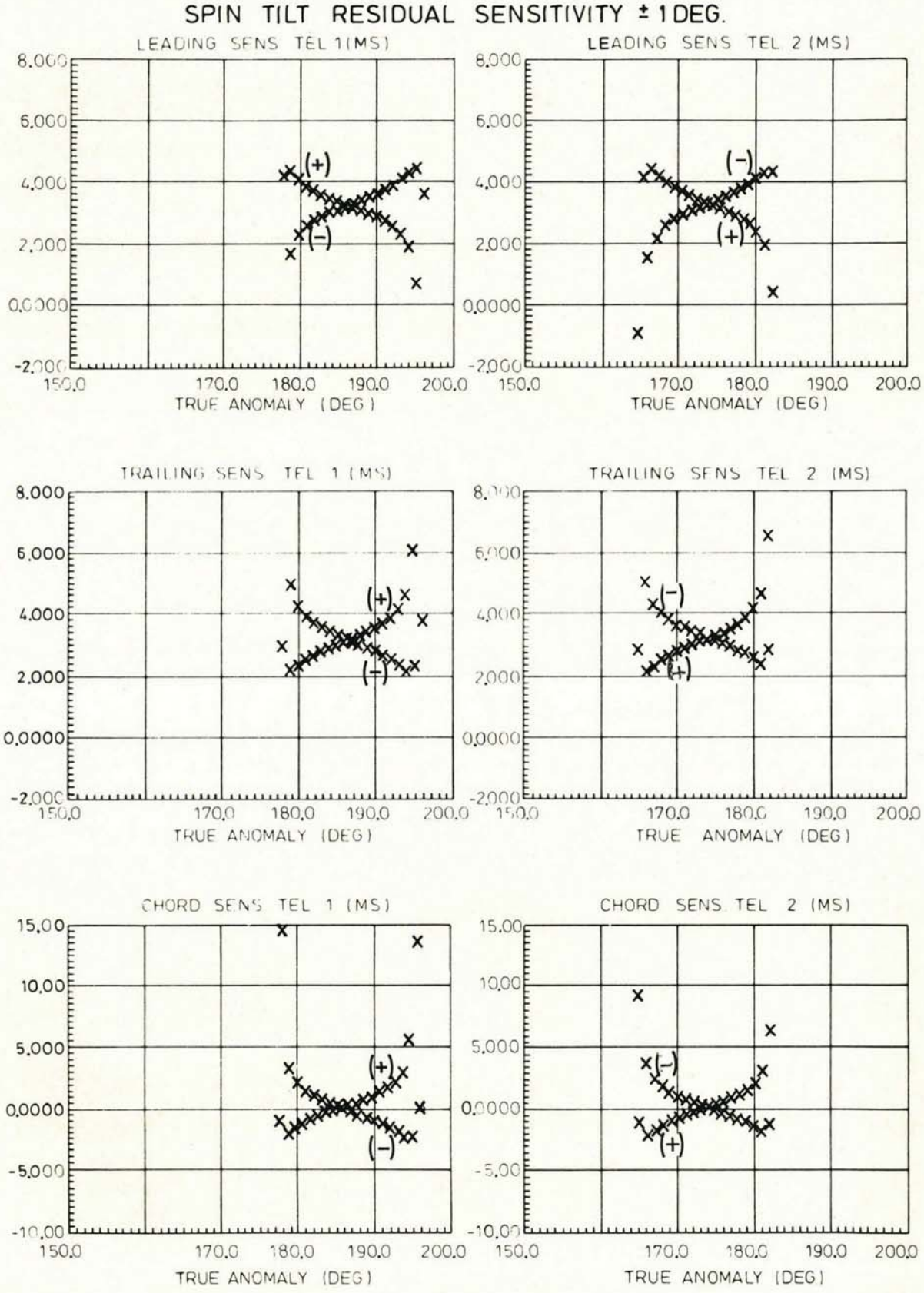
SPIN TILT RESIDUAL SENSITIVITY ± 1 DEG.
LEADING SENS TEL 1 (MS)
LEADING SENS TEL 2 (MS)
TRAILING SENS TEL 1 (MS)
TRAILING SENS TEL 2 (MS)
CHORD SENS TEL 1 (MS)
CHORD SENS TEL 2 (MS)
TRUE ANOMALY (DEG)
(+)
(-)

Figure 2.2.6

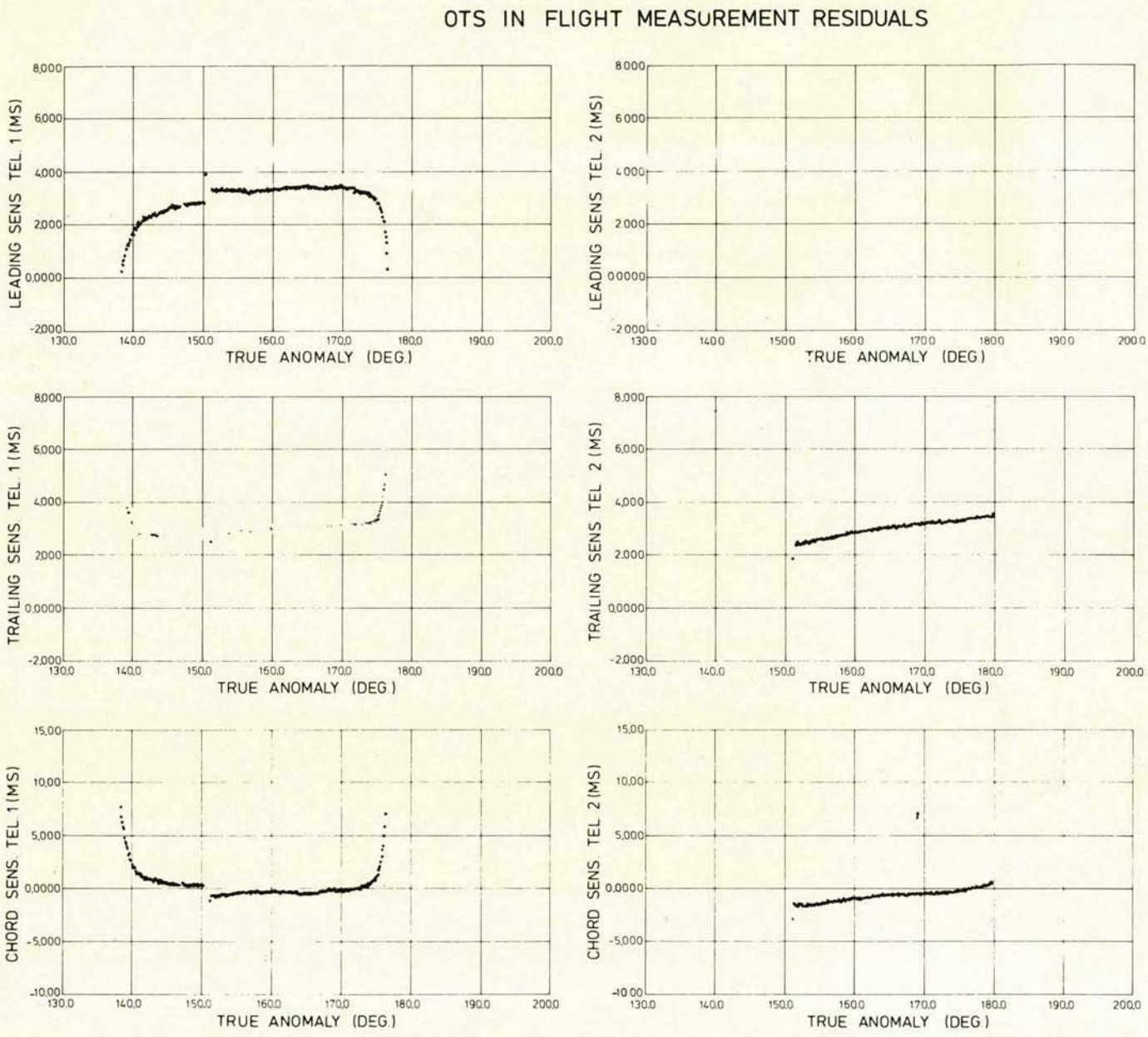
OTS IN FLIGHT MEASUREMENT RESIDUALS
LEADING SENS TEL 1 (MS)
LEADING SENS TEL 2 (MS)
TRAILING SENS TEL 1 (MS)
TRAILING SENS TEL 2 (MS)
CHORD SENS. TEL 1 (MS)
CHORD SENS. TEL 2 (MS)
TRUE ANOMALY (DEG.)

Figure 3.3.1

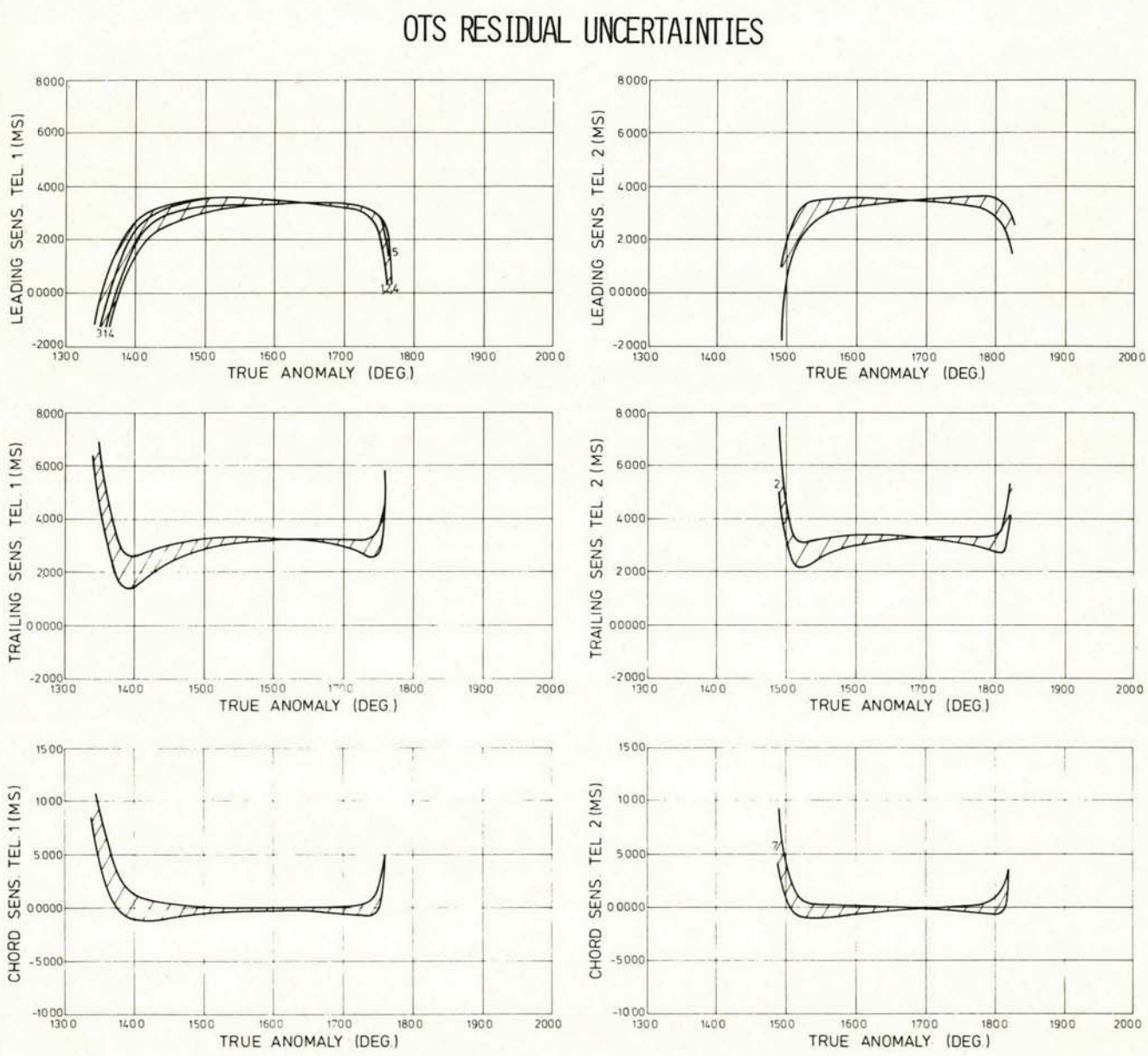
OTS RESIDUAL UNCERTAINTIES
LEADING SENS. TEL. 1 (MS)
LEADING SENS. TEL. 2 (MS)
TRAILING SENS. TEL. 1 (MS)
TRAILING SENS. TEL. 2 (MS)
CHORD SENS. TEL. 1 (MS)
CHORD SENS. TEL. 2 (MS)
TRUE ANOMALY (DEG.)

Figure 3.3.2

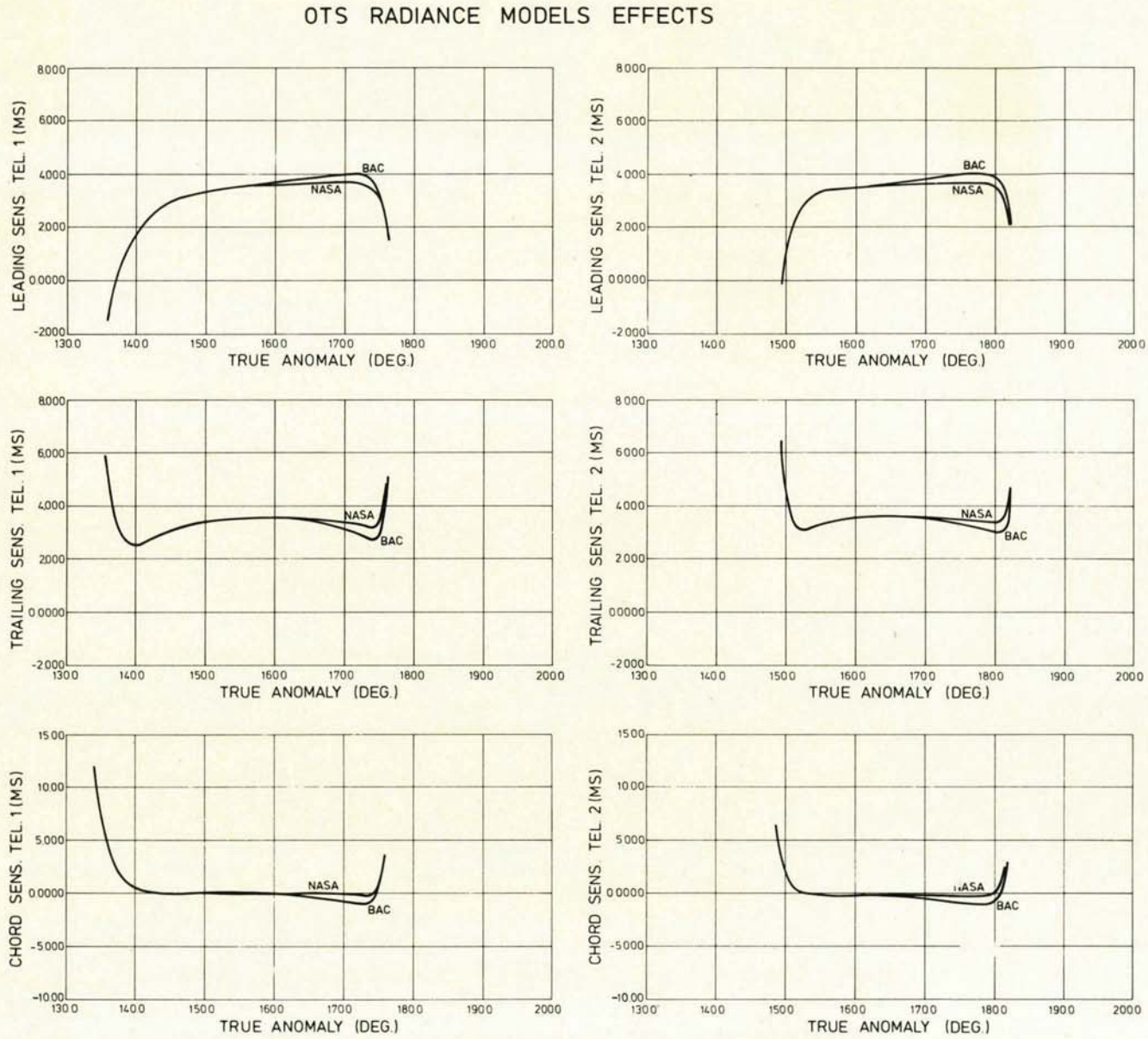
OTS RADIANCE MODELS EFFECTS
LEADING SENS. TEL. 1 (MS)
LEADING SENS. TEL. 2 (MS)
TRAILING SENS. TEL. 1 (MS)
TRAILING SENS. TEL. 2 (MS)
CHORD SENS. TEL. 1 (MS)
CHORD SENS. TEL. 2 (MS)
TRUE ANOMALY (DEG.)
BAC
NASA

Figure 3.3.3

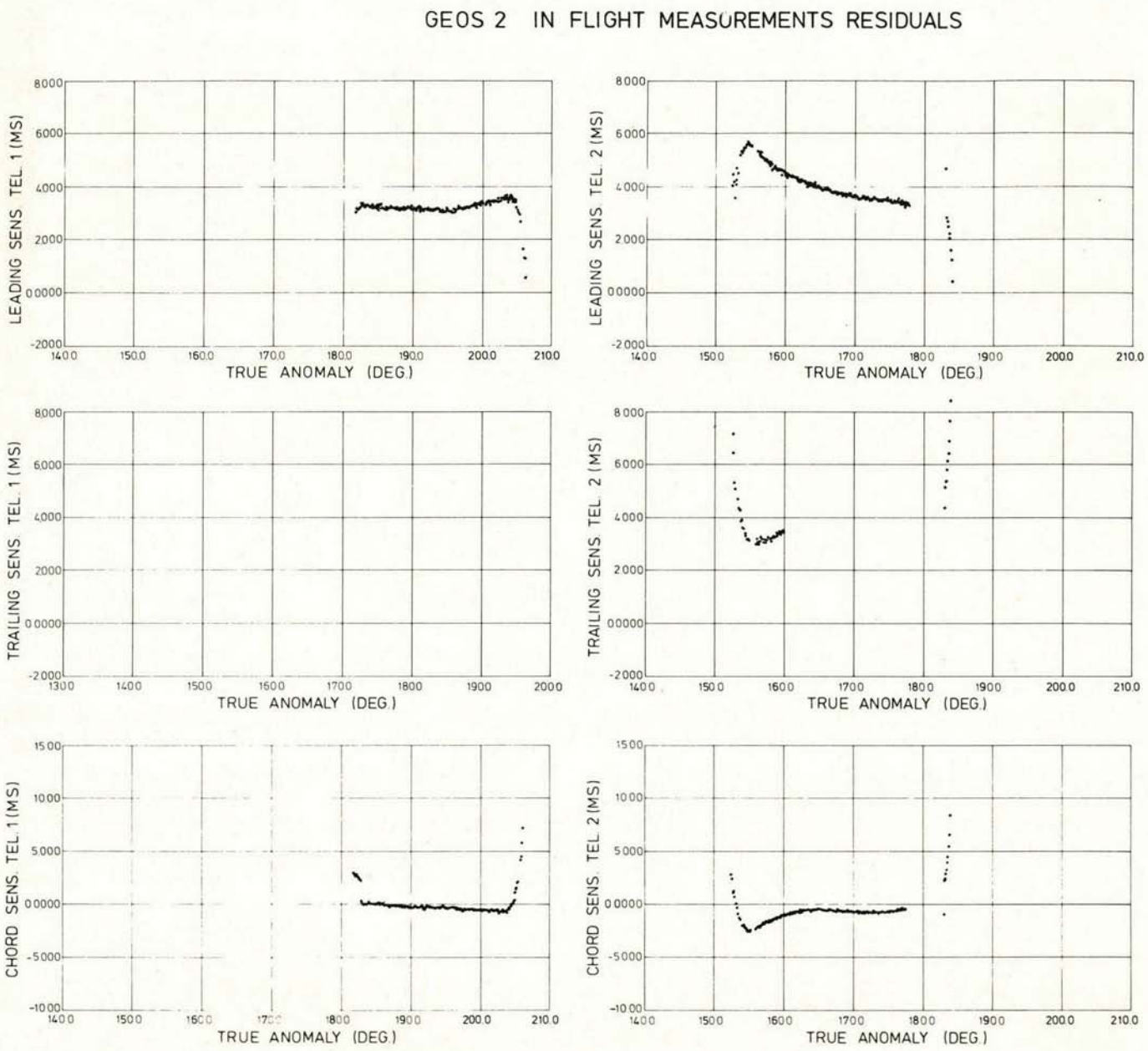
GEOS 2 IN FLIGHT MEASUREMENTS RESIDUALS
LEADING SENS. TEL. 1 (MS)
LEADING SENS. TEL. 2 (MS)
TRAILING SENS. TEL. 1 (MS)
TRAILING SENS. TEL. 2 (MS)
CHORD SENS. TEL. 1 (MS)
CHORD SENS. TEL. 2 (MS)
TRUE ANOMALY (DEG.)

Figure 3.4.1

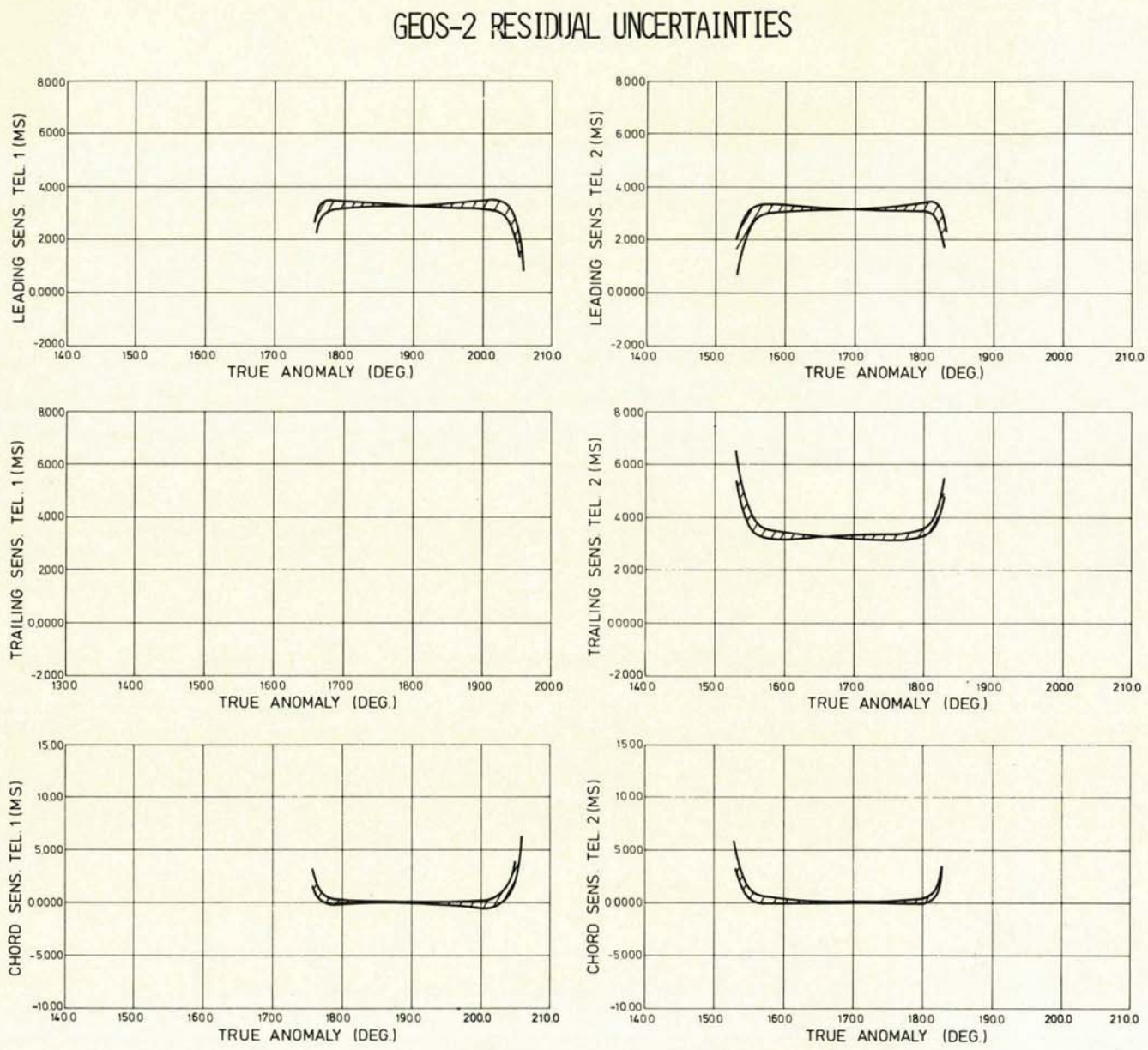
GEOS-2 RESIDUAL UNCERTAINTIES
LEADING SENS. TEL. 1 (MS)
LEADING SENS. TEL. 2 (MS)
TRAILING SENS. TEL. 1 (MS)
TRAILING SENS. TEL. 2 (MS)
CHORD SENS. TEL. 1 (MS)
CHORD SENS. TEL. 2 (MS)
TRUE ANOMALY (DEG.)

Figure 3.4.2

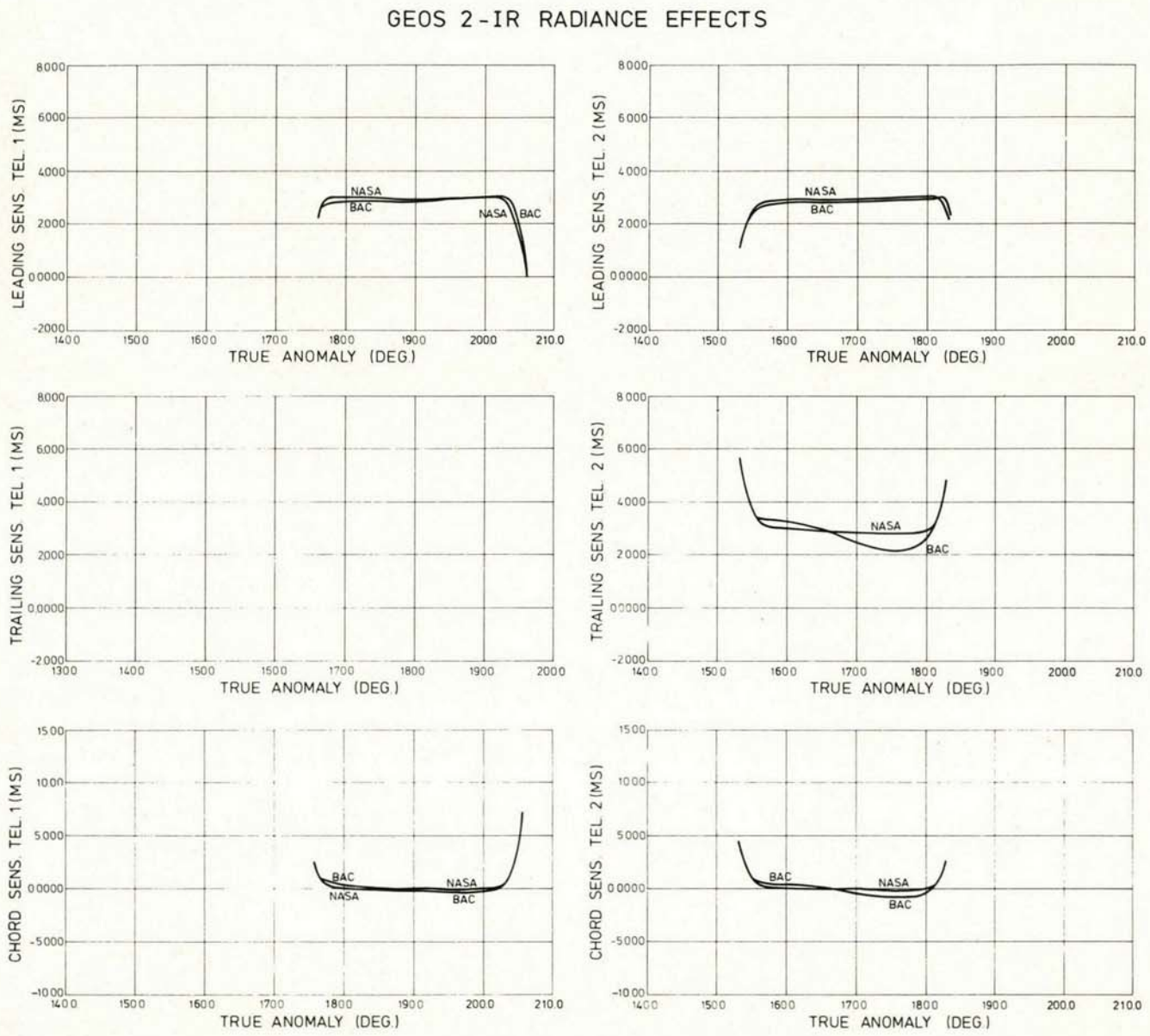
GEOS 2-IR RADIANCE EFFECTS
LEADING SENS. TEL. 1 (MS)
LEADING SENS. TEL. 2 (MS)
TRAILING SENS. TEL. 1 (MS)
TRAILING SENS. TEL. 2 (MS)
CHORD SENS. TEL. 1 (MS)
CHORD SENS. TEL. 2 (MS)
TRUE ANOMALY (DEG.)
NASA
BAC

Figure 3.4.3